

This work is on a Creative Commons Attribution 2.0 Generic (CC BY 2.0) license, <https://creativecommons.org/licenses/by/2.0/>. Access to this work was provided by the University of Maryland, Baltimore County (UMBC) ScholarWorks@UMBC digital repository on the Maryland Shared Open Access (MD-SOAR) platform.

Please provide feedback

Please support the ScholarWorks@UMBC repository by emailing [scholarworks-group@umbc.edu](mailto:scholarworks-group@umbc.edu) and telling us

what having access to this work means to you and why it's important to you. Thank you.

## Radio Loud AGN Unification: Connecting Jets and Accretion

Eileen T. Meyer<sup>1,2,a</sup>, Markos Georganopoulos<sup>2,b</sup>, Giovanni Fossati<sup>3</sup>, and Matthew L. Lister<sup>4</sup>

<sup>1</sup>Space Telescope Science Institute, 3700 San Martin Drive, Baltimore, MD 21218

<sup>2</sup>UMBC, 1000 Hilltop Rd, Baltimore, MD 21250

<sup>3</sup>Rice University, 6100 Main St, Houston, TX 77251

<sup>4</sup>Purdue University, 525 Northwestern Ave West Lafayette, IN 47907

**Abstract.** While only a fraction of Active Galactic Nuclei are observed to host a powerful relativistic jet, a cohesive picture is emerging that radio-loud AGN may represent an important phase in the evolution of galaxies and the growth of the central super-massive black hole. I will review my own recent observational work in radio-loud AGN unification in the context of understanding how and why jets form and their connection to different kinds of accretion and growing the black hole, along with a brief discussion of possible connections to recent modeling work in jet formation. Starting from the significant observational advances in our understanding of jetted AGN as a population over the last decade thanks to new, more sensitive instruments such as Fermi and Swift as well as all-sky surveys at all frequencies, I will lay out the case for a dichotomy in the jetted AGN population connected to accretion mode onto the black hole. In recent work, we have identified two sub-populations of radio-loud AGN which appear to be distinguished by jet structure, where low-efficiency accreting systems produce 'weak' jets which decelerate more rapidly than the 'strong' jets of black holes accreting near the Eddington limit. The two classes are comprised of: (1) The weak jet sources, corresponding to the less collimated, edge-darkened FR Is, with a decelerating or spine-sheath jet with velocity gradients, and (2) The strong jet sources, having fast, collimated jets, and typically displaying strong emission lines. The dichotomy in the  $\nu$ - $L$  plane can be understood as a "broken power sequence" in which jets exist on one branch or the other based on the particular accretion mode (Georganopoulos 2011). We suggest that the intrinsic kinetic power (as measured by low-frequency, isotropic radio emission), the orientation, and the accretion rate of the SMBH system are the fundamental axes needed for unification of radio-loud AGN by studying a well-characterized sample of several hundred Fermi-detected jets. Finally, we present very recent findings that the most powerful strong jets produce gamma-rays by external Compton rather than SSC emission, placing the origin of the IC emission in these strong jets at a radius inside the BLR and/or molecular torus (Meyer 2012).

### 1 Introduction

Blazars are understood to be end-on orientations of radio-loud AGN with broad-band spectral energy distributions (SEDs) dominated by the relativistic jet, consisting of synchrotron emission up to UV and X-ray, and inverse Compton (IC) emission at higher energies. This second, high-energy peak in the jet SED can be explained with both synchrotron-self Compton (SSC, in which the particles in the relativistic jet up-scatter synchrotron photons, [1, 2]) and external Compton (EC) models, in the latter case up-scattering photons from an external source, such as the broad line region [BLR; 3–5]). The very high apparent luminosities, significant polarization, and strong variability of blazars is explained by the same Doppler boosting that makes these sources the dominant population at high energies.

In the general unification scheme for radio-loud AGN, blazar-type sources are beamed (*i.e.*, jet face-on) counterparts to sources seen as Fanaroff and Riley radio galaxies [FR, 6]. The association of flat-spectrum radio quasars (FSRQ) with powerful FR IIs, and featureless BL Lac objects with FR Is was suggested chiefly by the correspondence in spectral types, morphologies, and range in extended radio luminosity [7]. However, violations to this scheme are well-known, *e.g.*, powerful, FR II-like BL Lacs, and low-power FSRQ [8–10], along with BL Lacs displaying SEDs, luminous narrow lines, and hot-spots typical of quasars [10, 11] and even broad lines in low continuum states [*e.g.* 12]. In addition, [13] discovered an apparently continuous anti-correlation between the synchrotron peak (and bolometric) luminosity ( $L_{\text{peak}}$ ) and the peak frequency ( $\nu_{\text{peak}}$ ), forming the now canonical 'blazar sequence' [13]. With blazars displaying a continuum in  $\nu_{\text{peak}}$  from low- to intermediate- to high- synchrotron peaking (LSP, ISP, HSP; we use roughly  $<14$ ,  $14-15.5$ ,  $>15.5$  in  $\log \nu_{\text{peak}}$ ), it was not clear how the SED appearance of

<sup>a</sup>e-mail: meyer@stsci.edu

<sup>b</sup>e-mail: georgano@umbc.edu

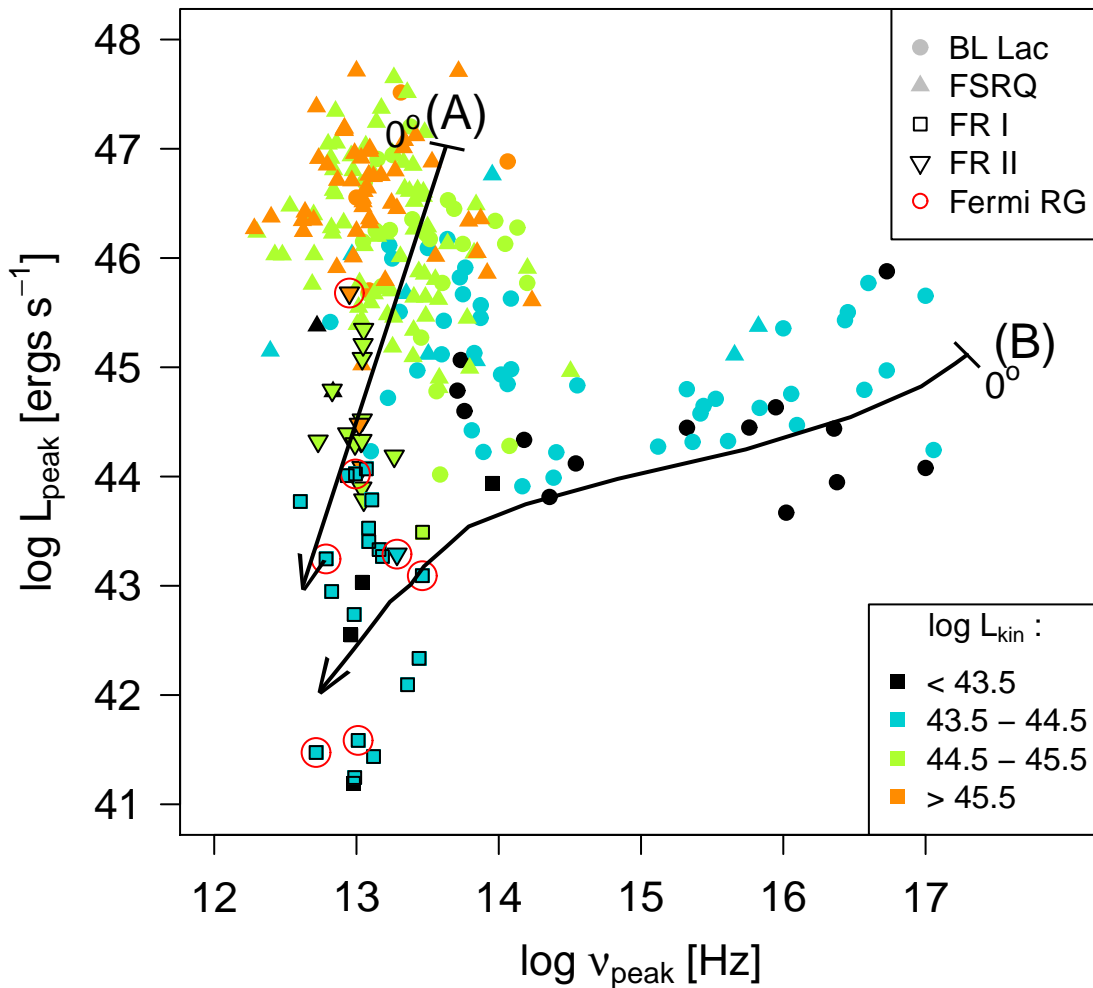


**Figure 1.** The synchrotron  $L_{\text{peak}} - \nu_{\text{peak}}$  plane. Using only well-sampled SEDs reveals a possible alternative to the continuous sequence, in which two populations show dramatically different behaviors in this plane. The branch at upper left is composed of strong-jet sources (typically powerful FSRQs), while the lower right branch consists of weak-jet sources (typically low-power BL Lacs). The debeaming path moving horizontally over the weak-jet sources is typical of a decelerating jet model characterized by velocity gradients. *Adapted from M11.*

blazars fit with the morphological dichotomy in the FR galaxies.

The blazar sequence has had several challenges. Indeed, [14] found that new sources they identified modify the blazar sequence to an envelope, with the area below the blazar sequence populated with sources. Similar envelopes were found by [15] and [16]. However, lower-luminosity sources appearing in the space below the blazar sequence were actually expected. If one takes the blazar sequence to be the rule for only the most-aligned (smallest orientation angle) sources, then progressively misaligned sources will experience less beaming and appear to form an envelope beneath the sequence.

The possibility for tracking similar jets as they filled the envelope motivated recent work [17, hereafter M11], in which we filled the synchrotron  $L_{\text{peak}} - \nu_{\text{peak}}$  plane using a much larger sample of well-characterized jet SEDs from sources over a wide range of orientations (from blazars

to radio galaxy jets imaged with high-resolution instruments). We tested whether the jet kinetic power ( $L_{\text{kin}}$ , as measured from the isotropic radio emission) could be the single parameter necessary for characterizing the jet SED, along with radio core dominance ( $R = \log L_{\text{core}}/L_{\text{ext}}$ ) as a measure of jet orientation (and therefore degree of beaming). *We found that the blazar sequence is actually broken into two populations in the  $L_{\text{peak}} - \nu_{\text{peak}}$  plane (Fig. 1).* The ‘weak’ jets (branch labeled ‘inefficient’) consist entirely of sources with  $L_{\text{kin}} < 10^{44.5}$  ergs  $\text{s}^{-1}$ , and extend from misaligned FR I radio galaxies at low  $\nu_{\text{peak}}$  up to well-aligned (as measured by  $R$ ) HSP BL Lacs. The ‘strong’ jets comprised a population of low  $\nu_{\text{peak}}$  jets (branch labeled ‘efficient’) which drop in  $L_{\text{peak}}$  rapidly with decreasing  $R$ .

This manuscript is organized as follows. In Section 2 we discuss the three (minimum) parameters that we believe necessary for radio-loud AGN unification, including a critical transition in accretion efficiency. In Section 3 we

show that the blazar divide of M11 is consistent with a *broken* power sequence with two branches. In Section 4 we briefly discuss the recurring issue of FSRQs masquerading as BL Lacs, and the potential pitfalls of dividing blazars by optical type only. Finally, in Section 5 we introduce the ‘Blazar Envelope’ as seen by *Fermi* and discuss the importance of the jet kinetic power and orientation of the jet in determining the gamma-ray luminosity. We also examine a recent finding suggesting that the high-energy emission of high-power jets is dominated by EC processes rather than SSC.

## 2 A Critical Accretion Rate?

Following M11, the important factors in RL AGN unification (*i.e.*, placing a source in Fig. 1) appear to be (a) the jet power  $L_{\text{kin}}$  (above  $10^{44.5}$  erg  $\text{s}^{-1}$ , one only finds sources on the strong-jet branch) and (b) the orientation angle (as proxied by radio core dominance in this case). However, there is a degeneracy at low  $L_{\text{kin}}$ , with sources appearing in both branches, which would imply that a third parameter is necessary (optical type is not reliable, as discussed in Section 4). Others have suggested that a critical accretion rate [19, 20], taking place at  $\dot{m} = \dot{m}_{\text{cr}} \sim 10^{-3} - 10^{-2} m_{\text{Edd}}$  [21, 22], and marking a transition from sources with inefficiently radiating accretion disks and therefore absent or weak broad emission lines (*i.e.*, BLL/FR Is) to sources with efficient accretion disks and strong broad emission lines (FSRQ/FR IIs), could explain the two distinct classes (optical/morphological).

In Fig. 2, we compare the estimated accretion rates for two sub-samples of the sources analyzed in M11 (*i.e.*, those in Fig. 1). The accretion rate  $\dot{m}$  is estimated from the ratio  $L_{\text{kin}}/L_{\text{Edd}}$ , where  $L_{\text{kin}}$  is the jet power scaled from low-frequency isotropic radio emission (M11) and  $L_{\text{Edd}}$  is the Eddington luminosity  $L_{\text{Edd}} = 1.3 \times 10^{38} (M/M_{\odot})$ . Black hole masses  $M$  were taken from the literature and averaged (further details will be discussed in a forthcoming paper). The two populations were carefully selected to correspond to strong-jet and weak-jet samples while minimizing contamination. To that end, the weak-jet sample was chosen from all sources with known synchrotron  $\log \nu_{\text{peak}}$  greater than 14.5, and the strong-jet sample was chosen from all sources with  $\log \nu_{\text{peak}} < 14.5$  and  $\log L_{\text{peak}} > 45.5$ . The latter cut was necessary to avoid potentially confusing LSP sources shown in the lower left of Fig. 1. Because sources on either branch, when misaligned, begin to coincide in this space, these sources were ambiguous in classification and omitted from the analysis.

As shown in Fig. 2, there does indeed appear to be a divide at  $-\log L_{\text{kin}}/L_{\text{Edd}} \sim 2-3$ . The weak-jet sources appear at lower accretion rates and the strong-jet sources at higher. Despite the fact that the errors on black hole masses and jet powers can be over half an order of magnitude, the divide in the populations is fairly distinct. Some have suggested that the accretion power merely gives an upper bound to  $L_{\text{kin}}$  [23]; this would then predict that the strong jet sources should have a significant population appearing at sub-critical efficiency as estimated for Fig. 2.

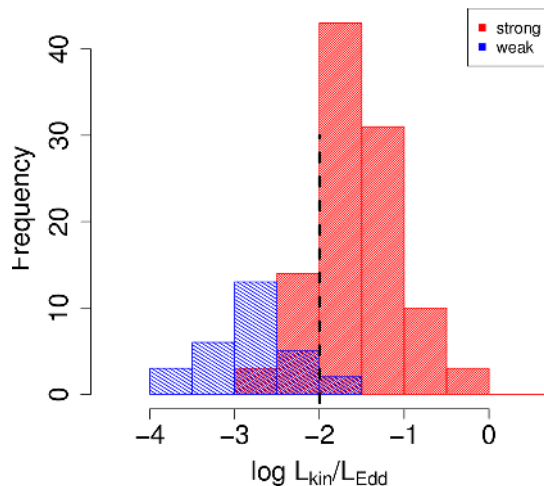


**Figure 2.** Histogram of estimated accretion rate ( $L_{\text{kin}}/L_{\text{Edd}}$ ) for a sample of blazars with known jet power and a reliable estimate of black hole mass. The sample is sub-divided into weak-jet sources (from Fig. 1, those with  $\log \nu_{\text{peak}} > 14.5$ ), and strong-jet sources (those with  $\log \nu_{\text{peak}} < 14.5$  and  $\log L_{\text{peak}} > 45.5$ ). Strong-jet sources have  $\log L_{\text{kin}}/L_{\text{Edd}}$  typically greater than critical values of -2 to -3 suggested in the literature, and thus this branch is labeled ‘efficient’ in Fig. 1; while weak-jet sources have sub-critical values and are labeled ‘inefficient’.

We suggest that a one-to-one correspondence is more in keeping with the results shown there, and that the accretion rate as measured by  $L_{\text{kin}}/L_{\text{Edd}}$  can be used as the third factor in AGN unification.

## 3 Exploring the new Broken Sequence

In M11, the new scheme was presented as a broken blazar sequence, with two broad groups, otherwise undifferentiated. We return to the synchrotron  $\nu_{\text{peak}} - L_{\text{peak}}$  plane to examine the possibility that a ‘blazar sequence’ remains within each of the two branches (*i.e.*, a strong sequence and a weak sequence).

**Building a Sequence.** For simplicity, consider all sources to have a black hole mass  $M \sim 10^9 M_{\odot}$ , and thus a fixed  $L_{\text{Edd}}$ . Sources that accrete at  $\dot{m} < \dot{m}_{\text{cr}}$  will have radiatively inefficient accretion disks. Assuming that the jet power cannot significantly exceed the accretion power, we require  $L_{\text{kin}} \leq \dot{m}L_{\text{Edd}} < \dot{m}_{\text{cr}}L_{\text{Edd}}$ . Sources that accrete at  $\dot{m} > \dot{m}_{\text{cr}}$  will have radiatively efficient accretion disks and  $L_{\text{kin}} < \dot{m}L_{\text{Edd}}$ . In both cases, given a set of sources with identical  $L_{\text{kin}}$ , the aligned ( $0^\circ$  orientation) sources will have the highest  $L_{\text{peak}}$  and  $\nu_{\text{peak}}$ . Because  $\nu_{\text{peak}}$  decreases as the radiative cooling becomes stronger, any situation where electrons in more powerful sources experience stronger radiative cooling will result to a *decreasing*  $\nu_{\text{peak}}$  with *increasing*  $L_{\text{kin}}$ , *i.e.*, a sequence. If we now gradually increase  $L_{\text{kin}}/L_{\text{Edd}}$ , the location of  $L_{\text{peak}} - \nu_{\text{peak}}$  for our  $0^\circ$  aligned source on the plot shifts to delineate a power sequence. The exact shape of this track depends on the physics of the jet. We consider below two plausible cases for the weak-jet and strong-jet populations separately.

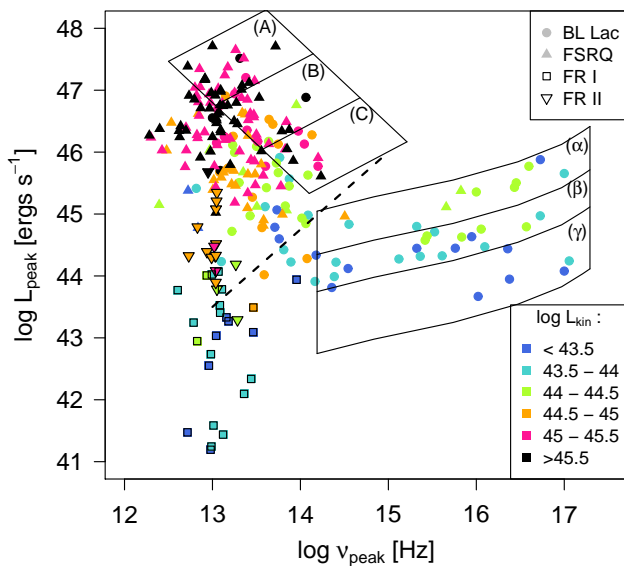


**Figure 3.** The blazar divide (same sources as in Figure 1) shown with overlaid ‘zones’ used to compare sources which are believed to have different intrinsic jet powers, based on the “broken power sequence” hypothesis. (See also Figure 4).

**The Inefficient Accretion Case.** We consider here the case in which the jet bulk Lorentz factor ( $\Gamma$ ) does not change as  $L_{kin}$  is increased, and  $L_{kin}$  scales linearly with the number density of relativistic electrons in the jet. In this case, and assuming that the electron energy distribution is  $n(\gamma) = k\gamma^{-p}$ ,  $p \leq 3$ ,  $\nu_{peak}$  is formed by the maximum energy electrons and remains fixed, while the peak luminosity increases linearly with the number density of relativistic electrons and, therefore, with  $L_{kin}$ . This is the line forming the upper right of the box for the inefficient branch in Fig. 1. Similar lines, possibly of different slope, are anticipated for other scenarios in which cooling increases with increasing  $L_{kin}$ . However, an important feature is that when  $L_{kin}$  increases enough that the source passes  $\dot{m}_{cr}$ , the inefficient accretion mode ceases being attainable. Interestingly, the highest  $L_{kin}$  sources in the inefficient accretion branch reach values of  $10^{44.5}$  erg s $^{-1}$ , which corresponds to  $\dot{m}_{cr} \sim 2.3 \times 10^{-3}$  for  $M = 10^9 M_{\odot}$ .

Does  $L_{kin}$  actually increase along the inefficient branch sequence? To evaluate this, we assume that the de-beaming tracks shown in Fig. 1 (curved lines defining the box at lower right) are a good representation of the actual de-beaming taking place. Keeping only HSP and ISP, we plot the distribution of  $L_{kin}$  in the three zones  $\alpha, \beta, \gamma$  in Fig. 4 (right panel). As expected, the average  $L_{kin}$  decreases as we move ‘down’ the sequence.

**The Efficient Accretion Case.** A plausible scenario for the strong-jet sources is that  $L_{kin}$  increases with  $\Gamma$ , as suggested by VLBI data [e.g. 10]. We assume in addition that the comoving energy density of electrons and magnetic field remain invariant. In this case,  $L_{kin} \propto \Gamma^2$ . Because the external photon field energy density in the comoving frame scales as  $U \propto U_{ext}$  and  $U_{ext}$  is not a function of

$\dot{m}$ , the cooling break in the electron distribution scales as  $\gamma_b \propto 1/U \propto \Gamma^{-2}$ . Then  $\nu_{peak} \propto B\gamma_b^2 \delta \propto \Gamma^{-3}$ , where we have used our assumption that  $B$  is fixed and our jet is aligned. Now  $L_{peak} \propto \Gamma^4$  for emission from plasma moving through a steady feature in the jet. Therefore, we have the sequence  $L_{peak} \propto \nu_{peak}^{-4/3} \propto L_{kin}^2$ .

To evaluate if  $L_{kin}$  indeed increases along the path shown, we considered the sources in boxes A, B, and C. The distribution of  $L_{kin}$  is shown for each box in the left panel of Fig. 4. As can be seen, the average  $L_{kin}$  increases from C to B to A, as expected.

## 4 A Caution on ‘False BL Lacs’

As noted by [24] and most recently [11, 25], there is a possibility that some broad-lined blazars appear as lineless sources (and therefore, are classified falsely as BL Lacs), due to the blazar jet being much brighter than any lines in the optical. This seems to require a combination of a source being (a) somewhat more beamed (so as to enhance the jet emission relative to the isotropic line emission) and (b) with a synchrotron peak which is at least near to the optical (*i.e.*, possibly, a lower-power source). In keeping with the idea of a half-sequence still existing in the strong-jet population, one would expect that more powerful sources have lower  $\nu_{peak}$  values, and brighter broad line spectra. Following aligned jets in the powerful branch from low to high  $L_{kin}$ ,  $\nu_{peak}$  will shift to lower energies and out of the optical, and the lines would come ‘up’, the source would be revealed as an FSRQ rather than BL Lac. The net effect, which we can readily test, should be that in moving ‘up’ the strong-jet sequence (red arrow in Fig. 1), the fraction of sources recorded as BL Lacs will drop. In fact this is seen in the left panel of Fig. 4, where we show BL Lac sources as the dark-shaded regions of the histogram. It is clear that in the progression from box C to B to A that the percentage of BL Lacs drops (58% to 24% to 15%), as expected if the broad lines of these sources are simply overcome by a bright jet in optical.

Further, we can check the effect of relative beaming on the proportion of BL Lacs in the strong-jet branch. Taking the scaling derived in Section 3, we can draw a line (with somewhat arbitrary normalization) corresponding to the sequence at 0 degree alignment (*e.g.*, the red line in Fig. 1). Selecting sources at moderate power ( $10^{43.5} - 10^{44.5}$  erg s $^{-1}$ ) to get a more uniform population (see M11), we can estimate the relative beaming by considering that a departure from the 0° line will follow a de-beaming path in the log-log plot with a slope of 4, *i.e.*, the relative beaming factor  $\delta/\delta_0$  can be estimated from the ratio  $\nu/\nu_0$ , where  $\nu_0$  is the frequency where the sequence and de-beaming path meet. As a source is found further from the red line, the smaller the value of  $\delta/\delta_0$ . As shown in Fig. 5, the fraction of BL Lacs falls from 100% in the highest bin of  $\delta/\delta_0$  down to 0%, which seems to support the idea that *beaming* is also an important factor in producing false BL Lacs.

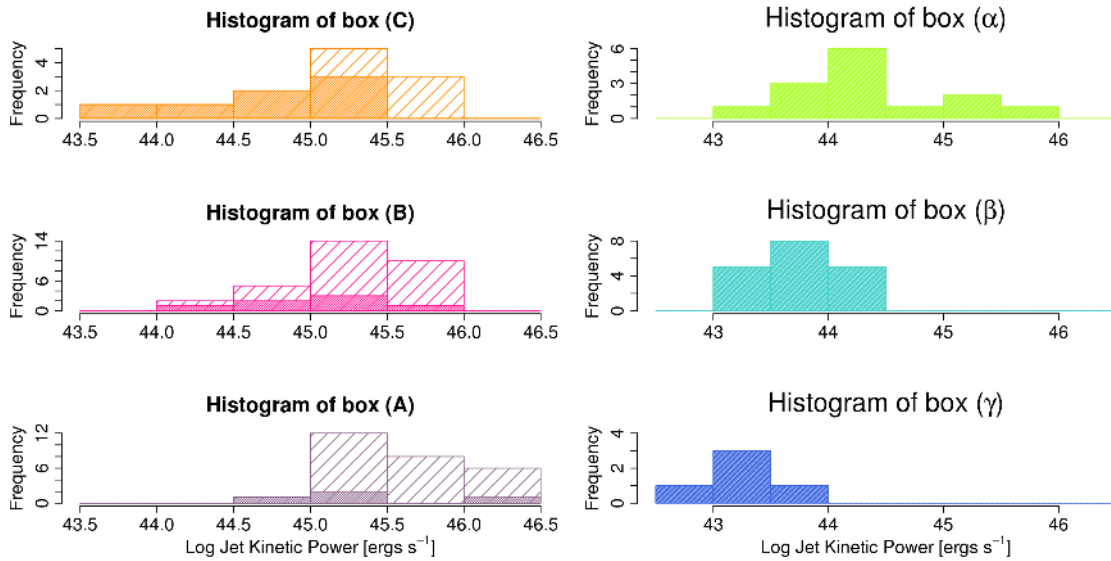


**Figure 4.** (Left) Distributions of  $L_{\text{kin}}$  for the boxes labeled A,B,C in Fig. 3. BL Lacs are shown as shaded regions. (Right) Distributions of  $L_{\text{kin}}$  for the boxes labeled  $\alpha,\beta,\gamma$  in Fig. 3. In both cases the predicted change in  $L_{\text{kin}}$  along a sequence is seen, supporting a ‘broken’ power sequence interpretation.

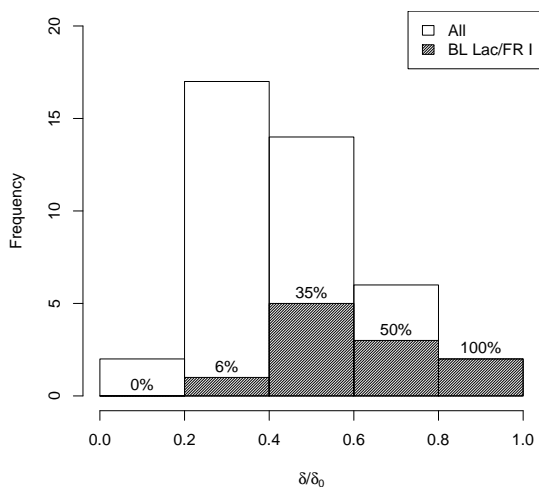


**Figure 5.** For moderate power ( $10^{43.5}-10^{44.5}$  erg  $\text{s}^{-1}$ ) sources in the strong-jet branch, we show the distribution of the relative beaming factor  $\delta/\delta_0$  as estimated from the position of the source relative to the sequence derived in Section 3. The shaded regions correspond to BL Lac sources. The fraction of BL Lacs falls off as beaming decreases, suggesting that these are false BL Lacs due to the jet emission covering the lines.

## 5 Fermi and the Blazar Divide

### 5.1 The Blazar Envelope at High Energies

Given that the trends shown in Fig. 1 appear to be driven by jet power and beaming (*i.e.*, orientation angle), it is natural to expect something similar to appear in the *inverse Compton*  $L_{\text{peak}} - \nu_{\text{peak}}$  plane. We show in Fig. 6 the

total LAT-band Luminosity (k-corrected) versus the LAT-band photon index ( $\Gamma$ ) for blazars in the second *Fermi* catalog [2FGL; 26]. While each of these measurements are very rough approximations for what we wish to measure (IC  $L_{\text{peak}}$  and  $\nu_{\text{peak}}$ , respectively), we still see a familiar trend: at low  $\Gamma$  values (corresponding to higher IC  $\nu_{\text{peak}}$ ), the gamma-ray luminosities are lower, suggesting again a zone of avoidance at high-peak, high-luminosity. The presence of two branches can not be readily discerned, but this may be in part due to the roughness of the estimators and particularly, the choice of the LAT-band integrated luminosity as a proxy for  $L_{\text{peak}}$ , as this will progressively underestimate sources peaking beyond the LAT band on either side (before for powerful FSRQ, and after for the HSP sources). It may also be due to the fact that the IC spectrum is not necessarily produced the same way for all sources (*i.e.*, the Compton dominance over synchrotron may vary).

An important feature in this figure is the location of the radio galaxies. As discussed above, we suggest that weak-jet sources are to be paired with FR I radio galaxies. As seen in Fig. 6, the FR I sources are found to have substantially softer LAT spectra than the ISP/HSP sources (marked with blue squares). This seems to match the horizontal trend discussed for Fig. 1, which can be explained if the jets have velocity gradients. On the other hand, the FR II radio galaxies seen with *Fermi* appear to have very similar IC peak frequencies to the strong-jet sources, consistent with a ‘simple’ jet as discussed in M11. In both cases a dotted line is shown connecting the average  $L_{\text{peak}}$ ,  $\nu_{\text{peak}}$  for the blazars and their respective parent population of radio galaxies.

In Fig. ??, we give a different view of the high-energy emission of blazars as seen with *Fermi*. Using a subsample of the 2FGL blazars with very good spectral cov-

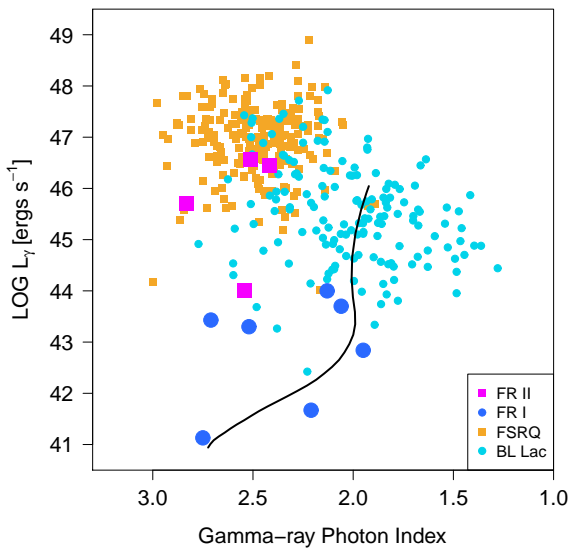


**Figure 6.** The Inverse Compton Envelope. Figure is adapted from [27]. The *Fermi*-detected AGN (large symbols) show that alignment plays a strong effect in the gamma-ray output. Interestingly, while the FR II sources appear to drop directly below the powerful FSRQ sources, FR I radio galaxies appear to follow a more horizontal track, similar to our findings in the synchrotron envelope (Fig. 1). The presence of a “forbidden zone” (empty region at upper right, implying no powerful, hard sources) suggests that there is a sequence in the IC plane, similar to that found in the synchrotron.

erage (in order to accurately fit a phenomenological model to determine the synchrotron/IC peaks), we show the average IC peak luminosity versus the radio core dominance at 1.4 GHz ( $R$ ). For the whole sample, there is no trend; however, when the sample is divided into bins of  $L_{\text{kin}}$ , the correlation between the peak  $L_{\gamma}$  and  $R$  ( $\log L_{\text{core}}/L_{\text{ext}}$ ) become significant within the bands. We have shown the OLS bisector fits for each bin as dashed lines (slopes range from 0.8 - 1.2, with positive Pearson’s  $r$  values from 0.4 - 0.8). The peak IC luminosity is strongly positively correlated with both the jet power and  $R$ , as we expect if these two factors are key to predicting jet phenomenology.

## 5.2 Diagnosing SSC versus EC with Populations

The high-energy emission in blazars can be explained with either SSC or EC emission. Generally low-power and lineless objects (*i.e.*, weak jets) are believed to radiate by SSC at high energies, while individually, many high-powered FSRQ (strong jets) have been more satisfactorily fit with EC models [28, 29]. However a consistent basis for which sources require EC has not been demonstrated for any particular class of blazars.

The location of the GeV emission is a matter of active debate, as it comes from locations close to the central engine that remain unresolved. However, identifying the nature of the radiation can give some insight. If the emission region is located within the sub-pc scale BLR, the GeV emission of blazars with strong lines should have

a strong EC component from up-scattered BLR photons [30]. However, if the region is several pc downstream (well outside the BLR/Molecular Torus) as suggested by some multiwavelength observations of variability [31, 32], EC is necessarily ruled out.

In Figure 7 we examine the relationship between Compton Dominance ( $CD$ , the log-ratio of IC and synchrotron  $L_{\text{peak}}$ ) and the radio core dominance,  $R$ , for a sample of 2FGL blazars. The black points are high-jet-power sources ( $\log L_{\text{kin}} > 45.5$ ), while the blue are low-power ( $\log L_{\text{kin}} < 43.5$ ). The flat distribution in the latter group may be consistent with the SSC models generally used to model these types of sources. For the high-power group, however, we find a significant trend of increasing Compton dominance with increasing radio core dominance (*i.e.*, alignment). *This can be interpreted as a signature of an EC process for a population of jets characterized by high kinetic powers.*

This statement can be explained as follows. The Doppler beaming factor,  $\delta$ , is a function of the Lorentz factor  $\Gamma$  and the orientation angle, and for monochromatic luminosities we have  $L = L_0 \delta^{3+\alpha}$ , where  $L_0$  is the rest-frame luminosity (at  $\delta = 1$ ), and  $\alpha$  is the energy spectral index at the frequency of interest. The exponent  $3+\alpha$  is the value assumed for a ‘moving blob’ in the jet. If the emission comes from a standing shock, the exponent would be  $2+\alpha$  [33].

In the case of emission by SSC, the IC peak has a beaming pattern which is identical to the synchrotron (*i.e.*, it follows the above equation). However, for EC models, the beaming at high energies goes as  $L_{\text{IC}} = L_{0,\text{IC}} \delta^{4+2\alpha}$  [34, 35]. The larger exponent indicates that as a source with significant EC emission is aligned, the IC peak should be more and more dominant over the synchrotron peak (*i.e.*,  $CD$  will increase with  $R$ . We can see that  $CD \propto \log(\delta^{1+\alpha})$ , and thus the dependence on  $\delta$  goes with an exponent of 2 when comparing the IC and synchrotron peaks (where  $\alpha = 1$ ). At radio frequencies, where the spectral index is confined to a fairly narrow range in values of  $\alpha_r = 0 - 0.5$ , the beaming exponent will be  $\sim 3 - 3.5$ . Thus an overall slope of  $\sim 2/3$ , up to 1 is expected in Fig. 7. While a more detailed investigation is in progress, we note that a higher slope might mean that the assumption that the Lorentz factor of the plasma emitting the gamma-rays is the same as that emitting at GHz frequencies is incorrect. While the current data shown are insufficient to put strong constraints on the slope, there is sufficient confidence in the positive correlation to say that EC is required for the most powerful strong-jet sources. Further, as shown in figure 8, the apparent velocities measured with VLBI support our interpretation of the trend in figure 7 as one related to increasing alignment giving rise to increased beaming: in such a case, the maximum apparent speeds ( $\beta_{\text{app}}$ ) should appear at intermediate angles of orientation, as at zero degrees no proper motions can be measured. As shown, this is exactly the pattern we see.

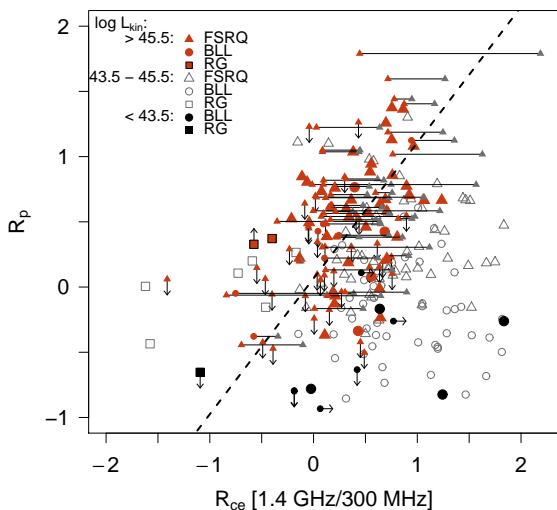


**Figure 7.** Inverse Compton dominance over synchrotron emission ( $L_{IC}/L_{sync}$ ) versus the radio core dominance  $R$ . We find that only for the strongest jets (orange), the inverse Compton dominance increases with increasing alignment, as measured by  $R$ , consistent with EC emission processes.

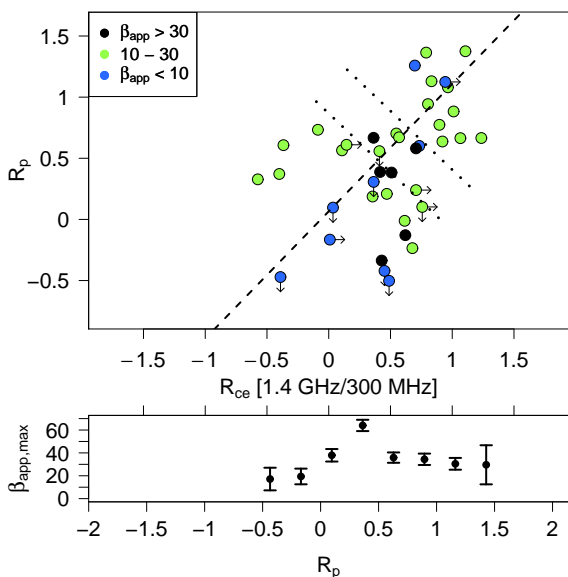


**Figure 8.** Inverse Compton dominance over synchrotron emission ( $L_{IC}/L_{sync}$ ) versus the radio core dominance  $R$ , with a color scale based on the apparent velocity measured with VLBI studies, when available from the literature. (Adapted from [18])

## 6 Conclusions

We have shown that the blazar sequence paradigm is in need of serious revision given the much more extensive blazar samples now available, and the increases in multi-wavelength SED coverage since the blazar sequence work was first published. We have shown that the blazar sequence may in fact be a “divide” in the  $L_{peak} - \nu_{peak}$  plane, with a “broken” power sequence still a possibility. We link this divide to a difference in accretion mode based on our estimates of efficiency using the low-frequency radio as a

proxy for jet power and black hole mass to estimate the Eddington rate. Finally, we have shown that only the most powerful sources show evidence for gamma-ray emission via the EC process.

## References

- [1] Maraschi, L., Ghisellini, G., & Celotti, A. 1992, *ApJ Lett.*, 397, L5
- [2] Marscher, A. P., & Travis, J. P. 1996, *A&As*, 120, 537
- [3] Ghisellini, G., & Madau, P. 1996, *MNRAS*, 280, 67
- [4] Błażejowski, M., Sikora, M., Moderski, R., & Madejski, G. M. 2000, *ApJ*, 545, 107
- [5] Sikora, M., Stawarz, Ł., Moderski, R., Nalewajko, K., & Madejski, G. M. 2009, *ApJ*, 704, 38
- [6] Fanaroff, B. L., & Riley, J. M. 1974, *MNRAS*, 167, 31P
- [7] Urry, C. M., & Padovani, P. 1995, *PASP*, 107, 803
- [8] Caccianiga, A., & Marchã, M. J. M. 2004, *MNRAS*, 348, 937
- [9] Landt, H., Perlman, E. S., & Padovani, P. 2006, *ApJ*, 637, 183
- [10] Kharb, P., Lister, M. L., & Cooper, N. J. 2010, *ApJ*, 710, 764
- [11] Ghisellini, G., Tavecchio, F., Foschini, L., & Ghirlanda, G. 2011, *MNRAS*, 414, 2674
- [12] Vermeulen, R. C., Ogle, P. M., Tran, H. D., et al. 1995, *ApJL*, 452, L5
- [13] Fossati, G., Maraschi, L., Celotti, A., Comastri, A., & Ghisellini, G. 1998, *MNRAS*, 299, 433
- [14] Padovani, P., Perlman, E. S., Landt, H., Giommi, P., & Perri, M. 2003, *ApJ*, 588, 128
- [15] Antón, S., & Browne, I. W. A. 2005, *MNRAS*, 356, 225
- [16] Nieppola, E., Tornikoski, M., & Valtaoja, E. 2006, *A&A*, 445, 441
- [17] Meyer, E. T., Fossati, G., Georganopoulos, M., & Lister, M. L. 2011, *ApJ*, 740, 98
- [18] Meyer, E. T., Fossati, G., Georganopoulos, M., & Lister, M. L. 2012, *ApJ Lett.*, 752, L4
- [19] Ghisellini, G., & Celotti, A. 2001, *A&A*, 379, L1
- [20] Ghisellini, G., Maraschi, L., & Tavecchio, F. 2009, *MNRAS*, 396, L105
- [21] Narayan, R., Garcia, M. R., & McClintock, J. E. 1997, *ApJ Lett.*, 478, L79
- [22] Narayan, R., & McClintock, J. E. 2008, *NAR*, 51, 733
- [23] Fernandes, C. A. C., Jarvis, M. J., Rawlings, S., et al. 2011, *MNRAS*, 411, 1909
- [24] Georganopoulos, M., & Marscher, A. P. 1998, *ApJ*, 506, 621
- [25] Giommi, P., Padovani, P., Polenta, G., et al. 2011, *arXiv:1110.4706*
- [26] Ackermann, M., Ajello, M., Allafort, A., et al. 2011, *ApJ*, 743, 171
- [27] Abdo, A. A., Ackermann, M., Ajello, M., et al. 2010, *ApJ*, 720, 912

- [28] Ghisellini, G., Tavecchio, F., Foschini, L., et al. 2010, MNRAS, 402, 497
- [29] Vercellone, S., Striani, E., Vittorini, V., et al. 2011, ApJ Lett., 736, L38
- [30] Sikora, M., Begelman, M. C., & Rees, M. J. 1994, ApJ, 421, 153
- [31] Böttcher, M., Reimer, A., & Marscher, A. P. 2009, ApJ, 703, 1168
- [32] Agudo, I., Marscher, A. P., Jorstad, S. G., et al. 2011, ApJ Lett., 735, L10
- [33] Lind, K. R., & Blandford, R. D. 1985, ApJ, 295, 358
- [34] Dermer, C. D. 1995, ApJ Lett., 446, L63
- [35] Georganopoulos, M., Kirk, J. G., & Mastichiadis, A. 2001, ApJ, 561, 111